50th AIAA Aerospace Sciences Meeting including the New Horizons Forum and Aerospace Exposition
09 - 12 January 2012, Nashville, Tennessee
AIAA 2012-0514

Preliminary findings from efforts to model pulsed inductive theta-pinch plasmas via Particle-In-Cell

Warner C. Meeks,[1] and Joshua L. Rovey[2]
Missouri University of Science and Technology, Rolla, Missouri 65409-0050

A method is pursued to approximately model the electron energy distribution of pulsed inductive plasma devices with Particle-In-Cell code to elucidate formation physics during early times (t < 1 μs). Specifically, reported results from AFRL-Kirtland's pulsed inductive device, FRCHX, are used as a test case to validate results. An *r-z* slab approximation is outlined and gyro-frequency, Larmor radius, and $\boldsymbol{E}\times\boldsymbol{B}$ guiding center drift are verified against theory to within 1% difference. The analyses presented, using both single electron and Particle-In-Cell modeling, agree with FRCHX reported results by showing that average electron kinetic energy does not exceed the ionization threshold of 15.47 eV for gaseous deuterium until after the first ¼ cycle of the ringing pre-ionization stage (when net magnetic field is approximately nullified). These results provide supportive evidence for the concept that bias field actually inhibits ionization if improperly implemented.

Nomenclature

e	fundamental charge	$t_{1/4}$	time to first ¼ of pre-ionization oscillatory cycle
f	device frequency	v_r	radial velocity
f_c	electron-cyclotron frequency	$v_{E\times B}$	$\boldsymbol{E}\times\boldsymbol{B}$ guiding center drift velocity
L	characteristic length of cylindrical reactor	v_θ	azimuthal velocity
m_e	electron mass	$v_\perp$	total velocity perpendicular to magnetic field the vector
R	characteristic radius of cylindrical reactor		
r_L	Larmor radius		

I. Introduction

PULSED inductive plasmas (PIPs) are becoming a staple of advanced electric space propulsion research. They provide a number of benefits over traditional electrode-activated propulsion plasmas and already have a well established research base in the fusion community. A number of PIP accelerators have been designed and bench-tested for electric propulsion (EP) applications including the Pulsed Inductive Thruster (PIT) developed by NASA and Northrop Grumman,[1,2,3] the Plasmoid Thruster Experiment (PTX) researched at Univ. of Alabama-Huntsville,[4] the Electrodeless Lorentz Force (ELF) thruster researched by Univ. of Washington,[5] the Experimental Coaxial Field Reversed Configuration Thruster (XOCOT) researched by the Air Force and Univ. of Michigan,[6] and the Faraday Accelerator with Radio-frequency-Assisted Discharge (FARAD) researched at Princeton's EPPDyL.[7] PIT has been investigated since the early 1980's by NASA and has seen multiple iterations and refinements. PIT devices are characterized by a planar coil geometry and a planar PIP current sheet formation and acceleration time of 10-20 μs. PTX, ELF, and FARAD create conical plasma current sheets by application of a conical coil geometry. This provides an inherent acceleration mechanism from an asymmetric magnetic field for the current sheet. A subset of PIPs known as field reversed configurations (FRCs), were initially researched as a means of imposing the necessary conditions for deuterium fusion without the large degree of complexity in hardware and in field topology associated with earlier compressively heated toroidal plasma fusion efforts.[8,9] However FRCs have come into a class all there own showing promise, not only in fusion but in high power space propulsion as well. FRCs are a PIP typically characterized by a high beta (plasma pressure / magnetic pressure ≅1) condition coupled with exclusively poloidal, self-consistent (i.e., closed-loop) magnetic fields. This topology is a more attractive (i.e., readily understood) alternative from spheromak type experiments which incorporate complicated radial and azimuthal components to there magnetic fields. The ELF thruster utilizes a rotating magnetic field (RMF) to prolong formation stability. Most FRC devices common in research today utilize what is known as the theta-pinch coil for

[1] Graduate Research Student, Mechanical and Aerospace Engineering, wcm994@mst.edu, AIAA Student Member.
[2] Assistant Professor, Mechanical and Aerospace Engineering, roveyj@mst.edu, AIAA Senior Member.

pre-ionization and formation providing a relatively simplified hardware design. This is contrary to FARAD, PTX, and PIT devices which generally do not have a loiter time to promote peak ionization and refine plasma formation. XOCOT utilizes a ringing theta-pinch but additionally has a coaxial inner coil that assists in stabilizing the formation and compression processes. Typically, discharge frequencies of coaxial devices are an order of magnitude slower, ideally providing longer plasma refinement times and higher ionization fractions. Despite these efforts and the simplifications stated that make FRC PIPs appealing what continues to be poorly understood is the coupling between field dynamics and particle physics during early formation times (i.e., $<10^{-6}$ s).

Ringing theta-pinch devices utilize a relatively simple coil geometry to induce fields and create plasma. Usually consisting of a single-turn coil that wraps cylindrically around a gas while current, *I*, flows in a purely azimuthal direction and, ignoring end effects, induces a uniform, axial magnetic field, ***B***. Described by Faraday's law given in equation (1) when this axial magnetic field is increasing in time it in turn induces an electric field, ***E***, that opposes the increasing current. This process is illustrated in Figure 1 which shows a cut-away of typical theta-pinch operation during an initial current rise.

$$\text{Faraday's Law;} \quad \oint \vec{E}\cdot\vec{dl} = \frac{-d}{dt}\int \vec{B}\cdot\vec{dA} \qquad (1)$$

This current rise (and subsequent ringing time-domain profile) is essentially the result of a typically under-damped LRC circuit where the coil represents the principal inductance (L) and is driven by a large (10's to 100's of kV) capacitor bank (C).

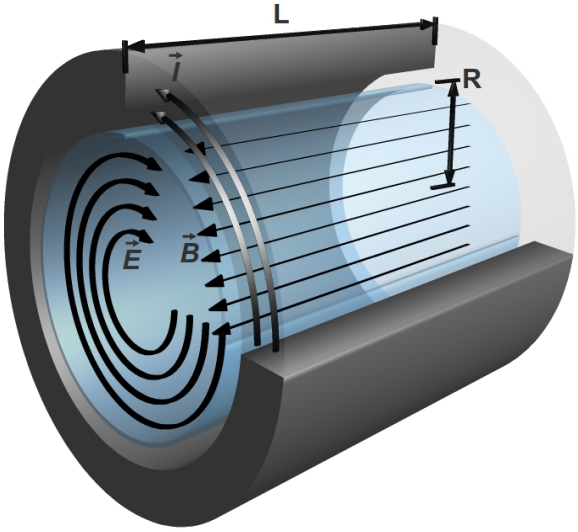

Figure 1: Ideal theta-pinch field topology for an increasing current, *I*.

II. Research Motivation

Since around the turn of the 21st century a collaborative effort between the Air Force Research Laboratory (AFRL) and Los Alamos National Laboratory (LANL) has focused on the use of FRCs to demonstrate feasible high temperature, high density, mass delivery systems for fusion applications. First from around 2000 to 2007 with the Field Reversed eXperiment – Liner (FRX-L) at LANL and then in 2007 constructing the Field Reversed Configuration Heating eXperiment (FRCHX) at AFRL-Kirtland. This initiative seeks to conduct FRC capture and compression studies with the primary goal of demonstrating magnetized target fusion.[11,12,10,13] Contrary to what present theory for pulsed plasma predicts, ionization is reported to form when the bias field has been approximately nullified (see Figure 2) by the first ring of the pre-ionization field when *dB/dt* approaches zero (i.e., when electric field is at its weakest).[10] This leads to an initial plasma formation with little to no trapped magnetic flux and this result is thought to reduce FRC lifetime. At present there is no good explanation for what is occurring during this early time and why there is a delay in plasma formation.

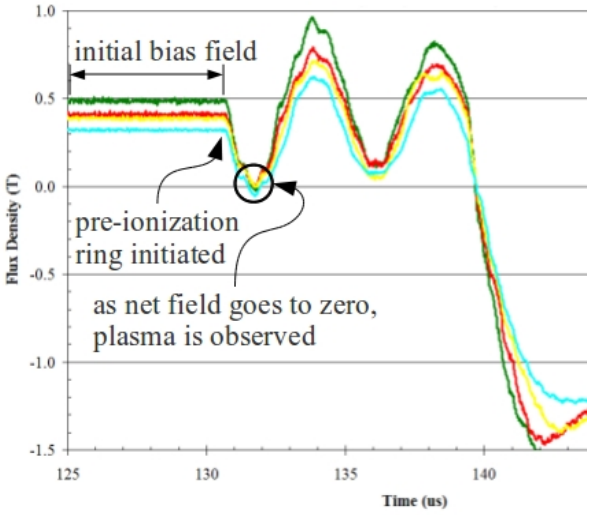

Figure 2: Reported magnetic field results (integrated B-dot probe data) from FRCHX (Ref 10).

To gain insight into the primary ionization mechanisms during this early time, interpreted magnet and electric fields and geometry from FRCHX are used as test case data for both a single electron and particle-in-cell study. These insights are meant to culminate into innovations in future PIP device designs to best utilize ionization mechanisms for early plasma formation.

III. Approach

A. Problem statement and assumptions

The freely available UniX based Object-Oriented Particle-In-Cell code, XOOPIC,[14,15] developed originally at U.C. Berkley is utilized to model ionization at early times in a deuterium gas for pseudo theta-pinch geometry. This code is a 2-D, relativistic, Monte Carlo collisional code that can be modeled electrostatically or, if curling electric fields lie only on the 2-D solution plane, can solve electrodynamic problems as well. Before ionization studies were undertaken efforts were made to ensure reasonable accuracy of the code and proper implementation of the particle physics. The geometry parameters used were a characteristic length of half the total length of FRCHX, or 18.2 cm and a constant radius of 6.5 cm. These parameters were chosen to capture the mid-section of a theta-pinch coil like FRCHX and provides a simulation length to diameter ratio, L/D=1.4. Three principle assumptions were used in one or both of the simulations and analyses presented here. These consist of; (1) fields present consist of only a uniform, axial magnetic field and an azimuthal electric field, (2) the problem is electrostatic over short time durations of less than 10 nanoseconds, and (3) fields are planar in a thin azimuthal slice. The field assumption, (1), simply implies that end effects (i.e., magnetic mirror, diverging electric fields) are ignored.

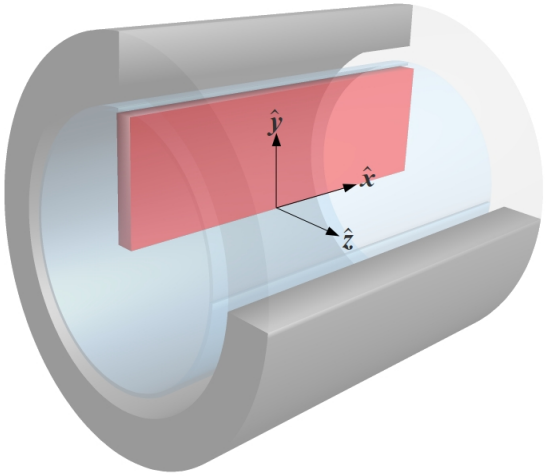

Figure 3: Azimuthal slice geometry simulated (red) using planar approximation.

The assumption of electrostatic conditions in a window of 10 nanoseconds for this study is facilitated by reported results of FRCHX (Figure (2)). In these results, during the first ¼ cycle of the pre-ionization ring, the magnetic field is seen to decrease sinusoidally from initial value of 0.5 Tesla to approximately zero in 1 μs. This corresponds well with a reported pre-ionization circuit frequency of 230 kHz ($t_{1/4} \approx 1.09$ μs). From here it is assumed that 10 ns << $t_{1/4}$ and subsequently $B(t) \approx B(t+10$ ns$)$. Additionally, the internal time-step used by the XOOPIC solver was assigned to be 1×10^{-12} s. This time-step falls well under the period of the largest gyro-frequencies seen of approximately 70.0×10^{-12} s.

The assumption of planar fields stems from a focus here on the use of a thin slice extending axially and radially as shown in Figure 3. While XOOPIC, a 2-D code, is able to natively run simulations in cylindrical coordinates the verifications described in this section as well as all following studies were performed using Cartesian coordinate approximation. This was done to avoid erroneous results from inputing azimuthal electric fields (i.e., $\nabla\times E\neq 0$) into an electrostatic solver. By extension, this assumption also implies the common use of azimuthal symmetry and ignores bulk motion azimuthally due to diamagnetic drifts as density becomes non-uniform.

B. Approximation of fields

To approximate field magnitudes seen in FRCHX with geometry as shown in Figure 1 and a sinusoidal magnetic field profile a simple ideal solenoid analysis is used along with Faraday's law to provide the connection between induced electric fields and time varying magnetic fields. Nomenclature for Faraday's Law in a theta-pinch device is depicted in Figure 4 for cylindrical coordinates. For uniform, orthogonal fields equation (1) is simplified to (2) and finally electric field magnitude can be approximated by equation (3).

$$2\pi r\cdot E=\left(\frac{-dB}{dt}\right)\pi r^2 \tag{2}$$

$$E=\left(\frac{-dB}{dt}\right)\frac{r}{2} \tag{3}$$

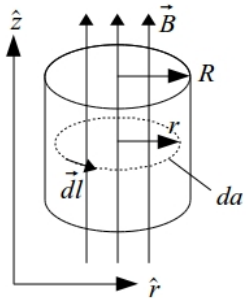

Figure 4: Application of Faraday's law to mid-section of theta pinch.

Magnetic field is modeled by an inverted sine function with positive offset matching initial bias of 0.5 Tesla. Device frequency, *f*, is approximated to be 250 kHz (frequency reported to be approximately 230 kHz in actual FRCHX test article[10]) yielding the appropriate ¼ cycle time of 1 μs.

$$B(t) = -0.5\sin(2\pi f t) + 0.5 \quad \text{(T)} \tag{4}$$

Applying equation (4) to (3) with a frequency, *f*=250 kHz, *B(t)* and *E(r,t)* in the mid-section of the theta-pinch coil are approximated by equation (5).

$$\begin{Bmatrix} \vec{B}(t) \approx -0.5\sin(1.57\times10^6 t) + 0.5 \;\; \hat{z} \;\; \text{(T)} \\ \vec{E}(r,t) \approx 392.7\, r \cdot \cos(1.57\times10^6 t) \;\; \hat{\theta} \;\; \text{(kV/m)} \end{Bmatrix} \tag{5}$$

Plots of these approximated field profiles can be seen overlaid with FRCHX results in Figure (5) for an ambiguous radial value. From here cylindrical coordinates are approximated to Cartesian coordinates by the nomenclature seen in Figure 3. For clarity this transition is also stated in equation (6).

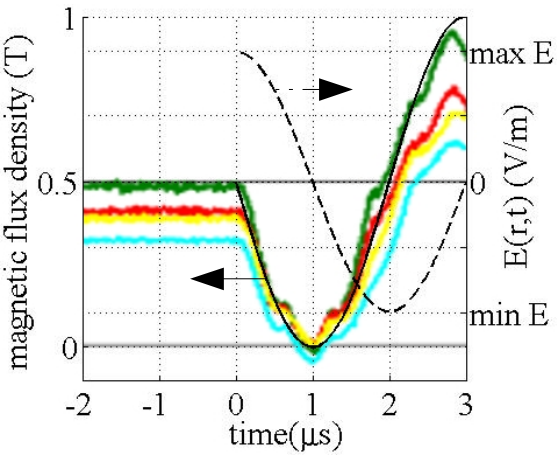

Figure 5: Reconstructed field profiles with original reported FRCHX results.

$$\begin{Bmatrix} B(t)\hat{z}_{cyl} \rightarrow B(t)\hat{x}_{cart} \\ E(r,t)\hat{\theta}_{cyl} \rightarrow E(y,t)\hat{z}_{cart} \end{Bmatrix} \tag{6}$$

C. Single particle modeling

Preliminary modeling of single particle kinetics in time-varying electric and magnetic fields was performed prior to simulation and analysis of the problem statement with XOOPIC. This initial approach serves two purposes. First it provides insights into the final state magnitudes that should be anticipated for the bounded geometry, multi-species simulations. Second, it provides an additional measure of verification for the XOOPIC code. In this study, the particle is not bounded at all and is free to move as fields dictate.

Single particle motion is modeled using equation (7) which simplifies to differential equations (8) and (9) for oscillatory motion in uniform orthogonal fields. The $\hat{y}$ and $\hat{z}$ directions here correspond to those depicted in Figure 3 and are re-iterated as being perpendicular to an axial magnetic field.

$$m\frac{d\vec{v}}{dt} = e\left(\vec{E} + \vec{v}\times\vec{B}\right) \tag{7}$$

$$\frac{d\vec{v}_y}{dt} = \left(\frac{e}{m_e}E_y \pm 2\pi f_c v_z\right)\hat{y} \tag{8}$$

$$\frac{d\vec{v}_z}{dt} = \left(\frac{e}{m_e}E_z \mp 2\pi f_c v_y\right)\hat{z} \tag{9}$$

Magnetic field starts at 500 mT and decreases sinusoidally to zero at 1 μs as seen for the FRCHX data. Because electron motion is unbounded for this single particle study, electric field is not varied with position as depicted in equation (5) and is instead fixed for a value of *y*=3.25 cm corresponding to a radial value in FRCHX of *R*/2. Thus *E(*3.25 cm*,t)* starts at a value of 12.76 kV/m and varies sinusoidally with time only, crossing zero at 1 μs as governed by equation (5).

D. Particle-In-Cell (PIC) code verification

Verification of particle kinetics in Cartesian coordinates is performed to verify unmodified PIC code with theory. These verifications include analysis of; (1) electron-cyclotron frequency, (2) Larmor radius, and (3) ***E***×***B*** drift velocity. Collisions were effectively turned off and no electric fields were prescribed, assigning only an initial azimuthal velocity. Tabulation of particle position by XOOPIC at each time step, in this case 1×10^{-12} seconds (0.001 nanoseconds), allows for re-construction of electron trajectory and subsequent extrapolation of both gyro-frequency and gyro-radius. Additional analysis of guiding center motion provides estimation of drift velocity.

Electron-cyclotron frequency is defined by equation (10)[16] for a uniform magnetic field magnitude, *B,* and

electron mass, m_e (≈9.11×10^{-31} kg). For a magnetic field of 0.1 Tesla the electron-cyclotron frequency is shown in Table 1 for both theory and simulation results yielding a percent difference of less than 1%.

$$f_{c\ theory} = \frac{e\,B}{2\pi\,m_e} \quad \text{(Hz)} \qquad (10)$$

Table 1: Verification of electron-cyclotron frequency for a 0.1 T magnetic field.

$f_{c\ theory}$ (equation 10)	2.79 GHz
$f_{c\ PIC}$	2.80 GHz
percent difference	0.36%

Larmor radius for electrons is defined via equation (11)[16] where $v_\perp$ is the total velocity perpendicular to the magnetic field. Initial particle velocity components were user specified as 8×10^6 m/s in the axial direction alone. Using this velocity and 0.1 T magnetic field in equation (11) and estimating simulated Larmor radius from XOOPIC output, r_L is obtained and reported in Table 2. Again percent difference between theory and simulation is less than 1%.

$$r_{L\ theory} = \frac{m_e v_\perp}{e\,B} \quad \text{(m)} \qquad (11)$$

Table 2: Verification of electron gyro-radius for 0.1 T magnetic field and initial velocity 8×10^6 m/s.

$r_{L,\ theory}$ (equation 11)	456 μm
$r_{L,\ PIC}$	460 μm
percent difference	0.88%

To verify proper ***E*×*B*** guiding center (GC) drift motion a uniform electric field orientated in the $\hat{z}$-direction (out of the slab) is applied to the above case providing a GC drift in the $\hat{y}$-direction. Here initial velocity is removed to allow for acceleration by the applied electric field only. For ***E*×*B***, GC drift velocity is defined via equation (12) which simplifies to equation (13) for orthogonal field vectors.

$$\vec{v}_{\boldsymbol{E}\times\boldsymbol{B}} = \frac{\vec{E}\times\vec{B}}{|\vec{B}|^2} \quad \text{(m/s)} \qquad (12)$$

$$v_{\boldsymbol{E}\times\boldsymbol{B}\ theory} = \frac{E}{B} \quad \text{(m/s)} \qquad (13)$$

Table 3: Verification of *E*×*B* guiding center drift velocity for 0.1 T magnetic field.

$v_{\boldsymbol{E}\times\boldsymbol{B},\ theory}$ (equation 13)	255.25 km/s
$v_{\boldsymbol{E}\times\boldsymbol{B},\ PIC}$	255.61 km/s
percent difference	0.14%

For a 25.525 kV/m applied electric field and 0.1 Tesla magnetic field the theoretical GC drift velocity is shown along with the estimated velocity from PIC simulation. As with gyro-frequency and Larmor radius, percent difference between theory and simulation vary by less than 1% again.

E. Iterative PIC scheme

Electrostatic solve is used for these studies because electric field curls azimuthally (i.e., in/out of the r-z plane). The iterative approach used for running XOOPIC was adopted out of the necessity to be able to completely control time-varying electric fields directed normal to the plane of simulation. This is not allowed natively in XOOPIC except for electrostatic fields. The iterative scheme in brief involves; (1) running XOOPIC for a short duration (i.e., 5-10×10^{-9} s) with zero initial electron velocity, (2) exiting XOOPIC and writing all electron/ion positions/velocities to file upon exit, (3) post-processing an average velocity for electrons, and (4) returning to step 1 with the calculated average electron velocity applied as the new initial electron velocity for all electrons in the system. In these studies ions created (which were very few, if any) are discarded, beginning each new iteration with the initial electron population of 10^{12} m^{-3} and zero ions. Any electrons lost to boundaries are not involved in post-processing and are reset (in terms of position) at the beginning of the next iteration.

IV. Results and Analysis

A. Single electron energy results

Figure 6 shows kinetic electron energy data for the applied fields shown in Figure 5. For an assumed initially "cold" electron, energy starts at zero and is seen to vary minimally until approximately 0.9 μs. By this time applied magnetic field has been reduced by nearly 99% from 500 mT to 6.2 mT. Just 37 nanoseconds after the magnetic field transitions through zero (i.e., t=1.037 μs) oscillatory electron energy crosses the gaseous D_2 ionization threshold, $I_{g,D2}$, of 15.47 eV. Following this, at approximately 1.05 μs, energy peaks at 32.2 V which corresponds to a velocity magnitude of 3.35×10^6 m/s. This time also corresponds to a field magnitude of 1.5 mT and when combined with the afore mentioned velocity yields a Larmor radius of 1.2 cm.

This simple analysis of single electron kinetics for orthogonal time-varying fields show that, from rest, the electron only achieves deuterium level ionization energies as magnetic field goes to zero. This agrees qualitatively with reported results of FRCHX. However in this simple analysis a single radial location was used thus ignoring the transition to higher electric field magnitudes as seen in a real device as electrons drift radially outward by $\boldsymbol{E}\times\boldsymbol{B}$ GC drifts. Also no boundary conditions were set to allow electrons to lose energy to the walls nor is a background gas present to allow energy loss via collisions as electrons approach the deuterium excitation energy (≈14.9 eV).

B. Iterative PIC results

Figure (7) shows results from the iterative PIC approach outlined above against the earlier single electron results. In these tests collisions are modeled however, do not play a major role because ionization level energies do not occur until $t > t_{1/4}$. Elastic collisions are also modeled and provide some dispersal of the energy distribution from a super-thermal, or near-beam profile. It can be seen from Figure (7) that the PIC approach follows a similar trend to that of the single particle approach and subsequently corresponds well with the FRCHX reported data. Referring to what is not similar, the PIC averaged electron energy appears to lag the single particle model at the $t_{1/4}$ (1 μs) time. This lag seems to be the cause of a further delay of energies crossing the $I_{g,D2}$ threshold of 15.47 eV to 72 ns after $t_{1/4}$. It should be noted that a deuterium collisional cross-section table was not natively available in XOOPIC and thus the table for gaseous diatomic hydrogen ($I_{g,H2}$ = 13.6 eV) was used as a substitute in these preliminary studies.

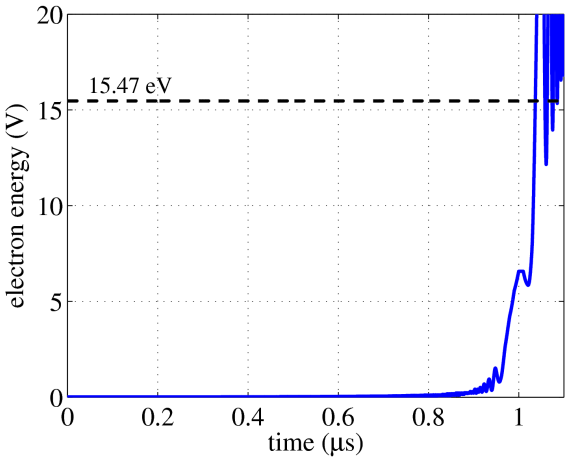

Figure 6: Kinetic energy for single electron energy study. Initially cold, u=0 m/s. Ionization threshold crossed at $t_{1/4}$+35 ns.

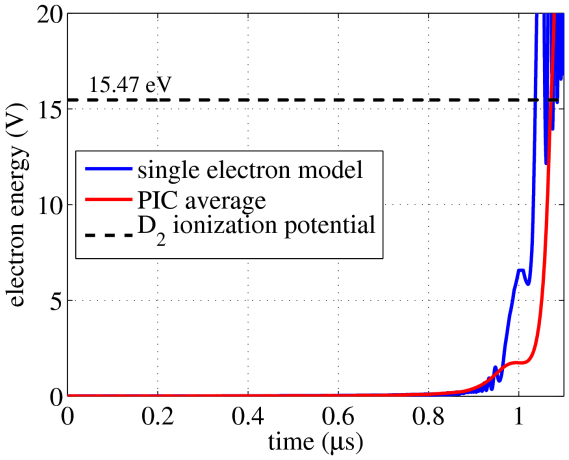

Figure 7: Iterative PIC kinetic energy results overlaid with single electron results. Ionization threshold crossed at $t_{1/4}$+72 ns for PIC results.

V. Conclusions

Based on analysis from both the single particle study and the iterative PIC study, as well as reported results from AFRL's FRCHX, ionization can actually be inhibited by the bias field if not properly matched with the pre-ionization field. Specifically, this refers to the matching of magnitudes between bias and PI fields. Furthermore, it is hypothesized that permitting the magnitudes of the net magnetic field and the electric field (proportional to dB/dt) to coincide within a small time deviation of each other results in poor ionization during the first ½ cycle of the pre-ionization oscillation.

VI. Future Work

Foreseen steps remaining for accurate FRCHX simulations via the iterative XOOPIC approach include; (1) proper implementation of boundary conditions, (2) accurate capture of particle-edge physics near the outer dielectric wall, and (3) input of collisional cross-section data for gaseous diatomic deuterium. Once accurate simulation is in place attention will be focused on describing the time evolution of the electron energy distribution and its profile classification. Specifically a better understanding of whether the distribution trends more towards a super-thermal (near-beam energy) or thermal (Maxwellian) distribution as it approaches ionization potential and when that occurs with respect to the ratio of electric to magnetic field magnitudes. Additional modeling of other theta-pinch devices, as well as PIP devices of differing geometries is also planned. Specifically, results from ELF[5], FARAD[7], and PIT[2] devices are of interest and will be the subject of further study.

VII. Acknowledgments

The authors would like to extend grateful thanks to the Air Force Office of Scientific Research (grant# FA9550-10-1-0204) and Dr. Mitat Birkan as well as the Missouri Research Board for their support of this work. Also, special thanks to David Kirtley (MSNW), Dan Brown (AFRL), Carrie Hill (AFRL), and Scott Kovaleski (Univ. of Missouri - Columbia) for sharing their insights and experiences involving PIP devices over the course of this research.

References

[1] Polzin, K.A., "Scaling and Systems Considerations in Pulsed Inductive Plasma Thrusters," *IEEE - Transactions on Plasma Science*, IEEE, Vol. 36, No. 5, pp. 2189-2198, 2008

[2] Polzin, K.A., "Comprehensive Review of Planar Pulsed Inductive Plasma Thruster Research and Technology," *J. Propuls. Power*, AIAA, Vol. 27, No. 3, p. pp. 513-531, May-June 2011

[3] Frisbee, R.H., & Mikellides, I.G., "The Nuclear-Electric Pulsed Inductive Thruster (NuPIT): Mission Analysis for Prometheus," *41st Joint Propulsion Conference and Exhibit*, AIAA, Tucson, AZ, 2005.

[4] Koelfgen, S.J., & Hawk, C.W., "A Plasmoid Thruster For Space Propulsion," *39th Joint Propulsion Conference and Exhibit*, AIAA, Hustsville, AL, 2003.

[5] Slough, J., Kirtley, D., & Weber, T., "Pulsed Plasmoid Propulsion: The ELF Thruster," *31st International Electric Propulsion Conference*, ERPS, Ann Arbor, MI, 2009.

[6] Kirtley, D.E., "Study of the Synchronous Operation of an Annular Field Reversed Configuration Plasma Device," Dept. of Aerospace Engineering, Univ. of Michigan, Ann Arbor, MI, 2008

[7] Choueiri, E.Y., & Polzin, K.A., "Faraday Acceleration with Radio-Frequency Assisted Discharge," *J. Propuls. Power*, AIAA, Vol. 22, No. 3, pp. 611-619, 2006

[8] Tuszewski, M., "Field Reversed Configurations," *Nuclear Fusion*, IAEA, Vol. 28, No. 11, pp. 2033-2092, 1988

[9] Steinhauer, L.C., "Review of field-reversed configurations," *Physics of Plasmas*, AIP, Vol. 18, No. 7, , 2011

[10] Grabowski, C., Degnan, J.H., Amdahl, D.J., et. al., "FRC Lifetime studies for the field reversed configuration heating experiment (FRCHX)," *53rd Plasma Physics Meeting*, APS, Salt Lake City, UT, 2011.

[11] Taccetti, J.M., Intrator, T.P., Wurden, G.A., et. al., "FRX-L: A field-reversed configuration plasma injector for magnetized target fusion," *Rev. Sci. Instrum.*, AIP, Vol. 74, No. 10, , 2003

[12] Grabowski, C., Degnan, J., Babineau, M., et. al., "FRC compresion Heating Experiment (FRCHX) at AFRL," *Pulsed Power Conference*, IEEE, Albuquerque, NM, 2007.

[13] Wurden, G.A., Intrator, T.P., Zhang, S.Y., et. al., "FRC plasma studies on the FRX-L plasma injector for MTF," *Fusion Energy Conference*, IAEA, Vilamoura, Portugal, 2004.

[14] Verboncoeur, J.P., Langdon, A.B., & Gladd, N.T., "An object-oriented electromagnetic PIC code," *Comp. Phys. Comm.*, Elsevier Sci., Vol. 87, No. , , 1995

[15] Verboncoeur, J.P., "Particle simulation of plasmas: review and advances," *Plasma Phys. Control. Fusion*, IOP, Vol. 47, No. 5A, , 2005

[16] Chen, F.F., "Introduction to Plasma Physics and Controlled Fusion," 2nd ed., 2006, Springer, p. 181, 185-186, 206